

A Three-dimensional Coupled Thermo-hydro Model for Enhanced Geothermal Systems

S. N. Pandey*[‡]

* Department of Applied Mechanics, Indian Institute of Technology Madras, Chennai 600036, Tamil Nadu, India

[‡] S. N. Pandey, Department of Applied Mechanics, Indian Institute of Technology Madras, Chennai 600036, Tamil Nadu, India, Tel: +91 4422574074, Fax: +91 44 2257 4052, snpiitm@gmail.com

Received: 15.07.2016 Accepted: 22.09.2016

Abstract- A three-dimensional numerical model of coupled fluid flow and heat transfer in EGS reservoir is investigated. The model considers a single uniform fracture surrounded by a three dimensional low permeable rock matrix. The flow is imposed on a fracture plane, consisting of a doublet system. The primary objectives of this paper are to analyze the effects of injection temperature and mass flow rates on heat extraction performances. The study results showed that for lower injection temperature heat extraction rates from the reservoir are higher. In case of higher injection mass flow rate, energy output increased significantly. However, after thermal breakthrough the energy output drops are seen faster in comparison of lower mass injection case. The faster energy drop with the time are result of the slower heat conduction inside the low permeable rock matrix perpendicular to the fracture. The present model neglected the fracture aperture evolution even though transmissivity reduction is observed. The transmissivity reduction is the results of flow resistance. The flow resistance inside the fracture is increased due to the non-laminar flow and cooling. The combined effect leads to rise the flow impedance of the reservoir. These effects are more for the higher mass at the lower injection temperature.

Keywords Enhanced geothermal systems, Coupled processes, Thermo-hydro effects, Heat extraction, flow impedance.

1. Introduction

Thermal energy stored inside the earth crust is known as geothermal energy. Geothermal energy is renewable, clean, ubiquitous, and has the potential of providing base-load power. During the last four decades, geothermal energy provides sustainable use for a large variety of applications, such as heating/cooling of buildings using ground source heat pump [1-3], desalination of water, industrial processes, mineral recovery, and electricity generation. From 2010 to 2014, the direct use of geothermal energy increased by 46.2% and reached 70,885 MWt [4]. The installed capacity of geothermal plants for electricity generation also increase by 17% in the past five year (2010-2015) and reached 12.729 MW [5]. The IEA (International Energy Agency) report says that by 2050, the share of geothermal energy expected to rise around 3.9% of energy for heat and 3.5% of electricity production [6].

There were several studies in past on nonisothermal fluid flow and heat transport in geothermal reservoir [7-13].

Jiang et al. [14] modeled the flow and heat transfer in EGS (enhanced geothermal system) reservoir. They considered the reservoir as homogeneous porous medium. Local thermal non-equilibrium approach was used. However, results of Jiang et al. [15] showed that temperature at production well was not much significantly affected when thermal equilibrium model assumption was used. Hadgu et al. [16] used FEHM (Finite Element Heat and Mass Transfer) to model the heat extraction in enhanced geothermal systems. Their results showed that fracture orientation with respect to the well-pair plane has significant influence on reservoir thermal drawdown. Fox et al. [17] studied the effect of fracture spacing on heat extraction performances. Their result shows that energy output increased with decreasing fracture spacing and increasing number of fractures in the reservoir. Kalinina et al. [18] examined the influence of the heterogeneities in sand-stone reservoirs. They showed that the impact of heterogeneities on the heat extraction or temperature drop was insignificant when the median fracture spacing was small, but heat extraction increased for larger median fracture spacing. They also demonstrated that the

heat extraction and temperature drop generally depend on the horizontal/vertical distribution of the permeability field and the fracture spacing. The sensitivity analysis in single variable aperture fracture was presented in [19]. The results of the study indicated that the heat transfer rate at the fracture matrix interface was apparently affected by the fracture aperture. Pandey et al. [20] studied the effect of correlation length on heat extraction from an EGS reservoir. The result shows that with smaller correlation lengths, heterogeneity did not significantly influence the temperature at the production well. But for large correlation lengths, significant temperature variation at production well due to strong flow channeling inside the reservoirs. The thermo-hydro simulations in fracture networks were studied in [21]. They used EPN (equivalent pipe network) approach to model the fracture network.

The present study develops a numerical model that fully couples the thermo-hydro processes during fluid injection and heat extraction from fractured EGS reservoir. The reservoir consider a single fracture connects the injection and production wells. The assumption is applicable for geothermal reservoir dominated by a single fracture/fault. The single fracture also provide useful insights behavior of individual fractures in a fracture network inside the reservoir. The present numerical approach and the insight from the simulated results are useful for geothermal reservoir engineering due to the lack of information available from field experiments and experience on long term behavior of EGS-type geothermal systems. The temperature and pressure dependent fluid properties such as density, viscosity, enthalpy are considered to calculate the energy output. Additionally, the effects of operating condition for long term performances of EGS reservoirs are also studied.

2. Governing Equations for Flow and Heat Transfer

The governing equations of fluid flow through fracture and the low permeable rock matrix can be expressed as [22-24]:

$$\mathbf{Q}_f = -\frac{b^3}{12\mu F_t} (\nabla P_f - \rho \mathbf{g}) \quad (1)$$

$$\mathbf{q}_r = -\frac{k}{\mu} (\nabla P_r - \rho \mathbf{g}) \quad (2)$$

where \mathbf{Q}_f (m^2/s) is the aperture integrated two-dimensional flux vector, b is the fracture aperture, P_f is the aperture-averaged pressure, P_r is the fluid pressure in the rock matrix, k (m^2) is the rock permeability, μ , ρ and \mathbf{g} are the dynamic viscosity, density of the water and gravitational

acceleration respectively. In present simulations, the flow rate near the wells is high enough that non-laminar effects are significant. To account for non-laminar effects, the experimentally motivated approach of Zimmerman et al. [25] is used. They proposed, $F_t = 1 + 0.00838\text{Re}$. The Reynolds number for flow is defined as $\text{Re} = (\mathbf{Q}_f \rho) / \mu$.

The governing equations for heat transport through the fracture and rock matrix are:

$$\frac{\partial (b(\rho c_p)_f T_f)}{\partial t} + \mathbf{Q}_f \cdot \nabla h_f - b \nabla \cdot (\lambda_f \nabla T_f) = f_T \quad (3)$$

$$\frac{\partial ((\rho c_p T)_r)}{\partial t} + \mathbf{q}_r \cdot \nabla h_r - \nabla \cdot (\lambda_r \nabla T_r) = 0 \quad (4)$$

where T is the temperature, λ is the thermal conductivity, h is the enthalpy and c_p is the specific heat. The subscripts f and r referring for fluid and rock, respectively. The local thermal equilibrium approached is used for the heat transport. In the present model, the permeability of rock matrix is much smaller than fracture, the heat transport through rock matrix is only dominated by conduction (advection term in eq. 4 is usually negligible). In eq. 3, f_T is the heat exchange term which is coupled at the fracture–matrix interface.

3. Numerical Method

The fluid flow and heat transport equations were solved numerically by using FEHM code (Finite Element Heat and Mass Transfer) [26]. FEHM is a well-verified CVFE (control volume finite element) code, designed to solve conservation of mass, momentum and energy equations (Eqs. 1, 2, 3 and 4) for non-isothermal single/multiphase flow through porous media. The details of solving the governing equations and method is given in ref. [27]. Simulations were conducted in a fracture–matrix system involving transport of fluid in a highly permeable horizontal fracture inside a 3-D geothermal reservoir. For modeling flow and heat transport in fracture, fracture is considered as an equivalent porous medium. The same approach was earlier used for Thermo-Hydro-Chemical modeling of geothermal system [9, 20].

4. Computational Domain and Boundary Conditions

The conceptual domain of geothermal reservoir is shown in Fig. 1. The size of reservoir is $1.5 \text{ km} \times 1.5 \text{ km} \times 1 \text{ km}$ in the x, y and z direction. The computational domain extends from 2 km to 3 km below the ground. The fracture in the reservoir is located 2.8 km below the top surface. The

temperature gradient $0.70\text{ }^{\circ}\text{C/m}$ is used to define the initial temperature distribution inside the reservoir. Hence, the temperature of water inside the fracture is initially $226\text{ }^{\circ}\text{C}$, while along the vertical boundaries zero heat (adiabatic) and mass flux (no flow) boundary conditions are specified. The average initial temperature at the ground surface of reservoir is considered $30\text{ }^{\circ}\text{C}$. The pore pressure inside the reservoir follow the natural pressure distribution with the depth with an assumption of no regional flow and tectonics activity. The initial pressure due to pore pressure gradient at the fracture locations at a depth of about 2.8 km is about 28 MPa . For efficient and accurate solution of the coupled thermo-hydraulic problem, a nonuniform but structured computational mesh is used. The computational meshes along $x-y$ and $x-z$ are shown in Figs. 2a and 2b, respectively. Since, the temperature and pressure gradients are very high below and above the fracture (i.e. sharp change in temperature and pressure profiles) very fine mesh are taken for $279.9 \leq z \leq 280.1$. For similar reason the computational mesh along $x-y$ plane is very fine near injection and production wells.

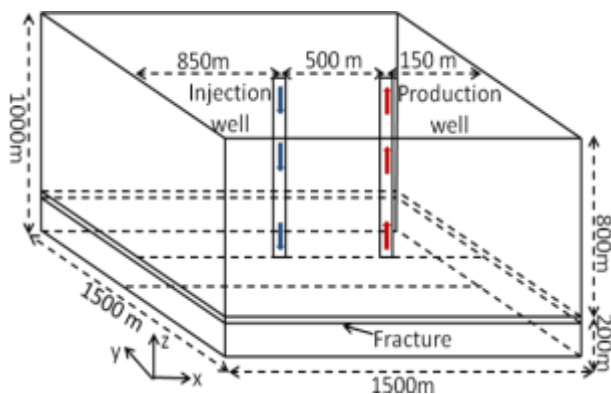


Fig. 1. Schematic diagram of a doublet geothermal heat extraction setup.

Table 1: Input parameters for numerical simulation [20].

Parameters	Value
Initial fracture aperture (m)	0.005
Reservoir permeability (m^2)	1×10^{-18}
Density of rock (kg/m^3)	2500
Heat capacity of water ($\text{J/kg/}^{\circ}\text{C}$)	4180
Heat capacity of rock ($\text{J/kg/}^{\circ}\text{C}$)	1000
Thermal conductivity of rock ($\text{W/m/}^{\circ}\text{C}$)	2.5
Thermal conductivity of water ($\text{W/m/}^{\circ}\text{C}$)	0.60

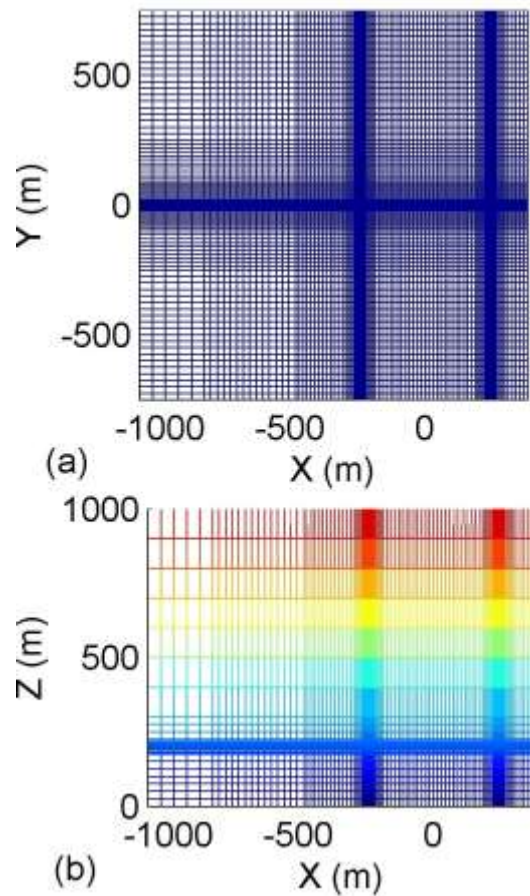


Fig. 2. Mesh generated in the study, (a) X-Y and, (b) X-Z direction.

Table 2: Injection scenarios.

Case No.	T_{inj} ($^{\circ}\text{C}$)	m_{inj} (kg/s)
1	60	40
2	80	40
3	60	60
4	80	60

5. Results and Discussion

Fully coupled thermo-hydro simulation of water injection into a nondeformable fractured geothermal reservoir have presented for the operational period of 20 years durations. To study the effect of injection mass flow rate and temperature, four cases have been considered. These are tabulated in Table 2. Two different values of fixed mass flow rates (40 and 60 kg/s) and two different values of injection temperature (60 and $80\text{ }^{\circ}\text{C}$) are considered. The values reservoir parameters are listed in Table 1. The results

pertaining to cooling of reservoir with time and production temperature drawdown are presented. The heat extraction during circulation of water in a doublet system can be expressed as follows:

$$\dot{E} = \dot{m}(h_{pro} - h_{inj}) \tag{5}$$

where \dot{m} is the production mass flow rate, h_{inj} and h_{pro} are the enthalpy of water at the injection and production well respectively. However, due to increase of injection pressure, enthalpy of injected fluid varied from 277 kJ/kg at beginning of injection to 292 kJ/kg at end (20 years) of the production for Case 1 injection condition (40 kg/s and 60 °C). Since enthalpy is a function of pressure and temperature ($h = f(P, T)$), and these effects are considered for calculation of heat extraction. From the second law of thermodynamics, conversion of heat to work is follow as:

$$\dot{m}(h_{pro} - h_{inj}) \left(1 - \frac{T_0}{T_{pro}}\right) \tag{6}$$

where T_0 and T_{pro} are the atmospheric temperature and the well head production temperature. Sanyal and Butler [28] proposed the following relation, is used in this analysis to calculate the electric power output based on an assumption that 45% of utilization efficiency of useful work is converted into electric power:

$$P = 0.45\dot{m}(h_{pro} - h_{inj}) \left(1 - \frac{T_0}{T_{pro}}\right) \tag{7}$$

where T_0 is the atmospheric temperature.

The water flow impedance I_R (MPa/(kg/s)) is calculate as:

$$I_R = \frac{P_{inj} - P_{pro}}{\dot{m}} \tag{8}$$

where P_{inj} and P_{pro} are the pressure at the injection and production well, respectively. The value of impedance parameter is inversely proportional to the fracture transmissivity. It is expected to be constant for nondeformable and nonreactive reservoir. However I_R has been seen to increase even for thermo-hydraulic modeling because increase of viscosity as the temperature of water inside the fracture decreases with time.

The evolution of temperature field and propagation of cold front inside the fracture are shown in Fig. 3 after 0.5, 2, 10 and 20 years from the beginning of injection for Case 1 injection condition. The temperature at the vicinity of the injection well drops very fast. The cold front (thermal front)

moving away from the injection well and reaches the production well. However the size of cold zone grows very

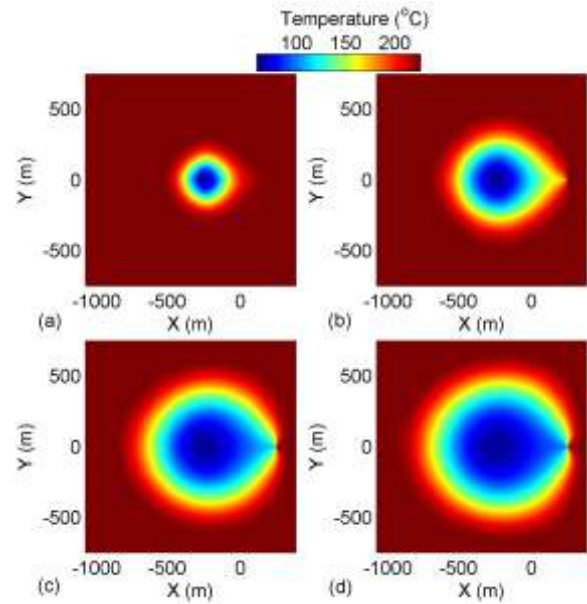


Fig. 3. The spatio-temporal evolution of temperature profile at the fracture plan ($z = 800$ m) for injection condition ($\dot{m} = 40$ kg/s and $T_{inj} = 60$ °C, (a) 0.5 year, (b) 2 years, (c) 10 years, and (d) 20 years.

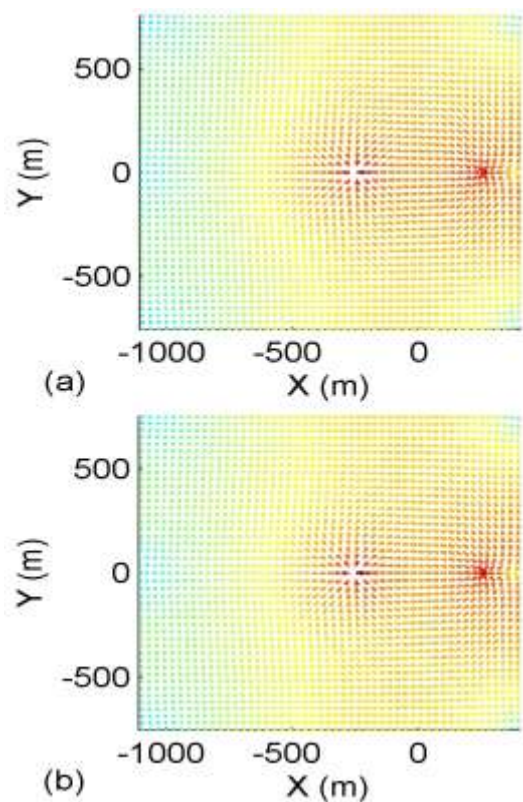


Fig. 4. Velocity vector plot at the fracture plan ($z = 800$ m) for injection condition ($\dot{m} = 40$ kg/s and $T_{inj} = 60$ °C, (a) 0.5 year, and (b) 20 years.

slowly after the arrival of cold front at production well. Since the heat transfer within the fracture is advection dominated, the cooling is mainly dictated the flow field. The flow field is shown in Fig. 4 in the form vector plot of aperture-integrated flux (Q_f). The colour of arrows represents the relative magnitude of flux. Additionally flux is indicated as larger if the colour varies from blue to red. The cooling between the wells is faster than other parts of the fracture as the cold water takes minimum time to reach the production well when travels linearly between wells. The flux vector plots in Figs. 4a and 4b look very similar. Since, the transmissivity reduction caused by flow resistance is very small and evolutions due to T-H-M-C processes are neglected.

The temperature distribution within the fracture surface after 20 years of operation for Case 1, Case 2, Case 3 and Case 4 are presented in Fig. 5. Among all the Cases, the more temperature drop occurred in Case 3 injection condition. This suggests that higher mass leads to higher advection inside the reservoir/fracture and water travels a longer distance within the fracture. In addition, temperature drop inside the reservoir is more sensitive to injection temperature. Figs. 5a and b shows the results of same injection mass flow rate but different injection temperature. These figures suggests that higher temperature injection leads to lower temperature drop inside the reservoir due to decrease the temperature difference between injected fluid and reservoir rock temperature. This leads to less cooling inside the reservoir.

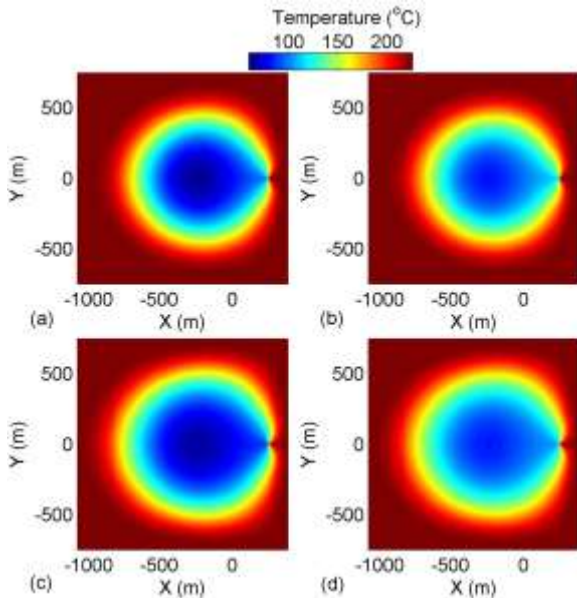


Fig. 5. Temperature field after 20 years at the fracture plan ($z = 800$ m) for different injection conditions: (a) $\dot{m} = 40$ kg/s and $T_{inj} = 60$ °C, (b) $\dot{m} = 40$ kg/s and $T_{inj} = 80$ °C, (c) $\dot{m} = 60$ kg/s and $T_{inj} = 60$ °C, and (d) $\dot{m} = 60$ kg/s and $T_{inj} = 80$ °C.

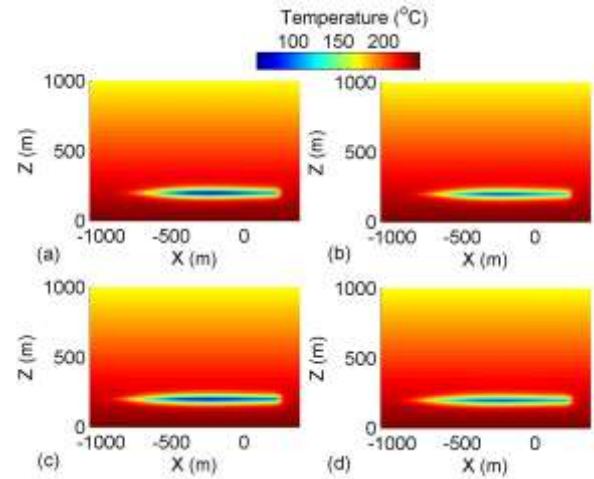


Fig. 6. Temperature distribution in the reservoir matrix after 20 years along the vertical section at the plane ($y = 0$), (a) $\dot{m} = 40$ kg/s and $T_{inj} = 60$ °C, (b) $\dot{m} = 40$ kg/s and $T_{inj} = 80$ °C, (c) $\dot{m} = 60$ kg/s and $T_{inj} = 60$ °C, and (d) $\dot{m} = 60$ kg/s and $T_{inj} = 80$ °C.

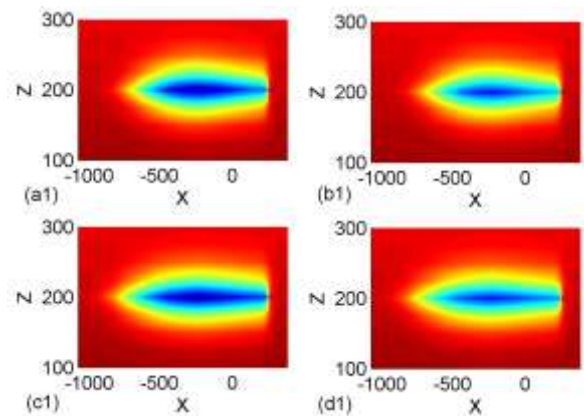


Fig. 7. The zoom views of temperature fields of Fig. 6.

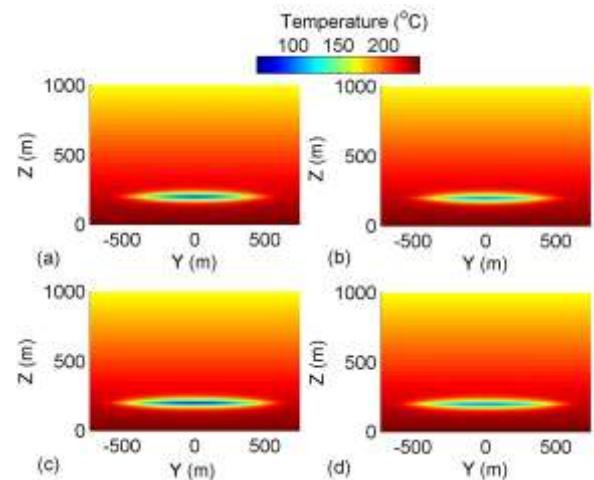


Fig. 8. Temperature distribution in the reservoir matrix after 20 years along the vertical section at the plane ($x = 0$), (a) $\dot{m} = 40$ kg/s and $T_{inj} = 60$ °C, (b) $\dot{m} = 40$ kg/s and $T_{inj} = 80$ °C, (c) $\dot{m} = 60$ kg/s and $T_{inj} = 60$ °C, and (d) $\dot{m} = 60$ kg/s and $T_{inj} = 80$ °C.

$^{\circ}\text{C}$, (c) $\dot{m} = 60 \text{ kg/s}$ and $T_{inj} = 60^{\circ}\text{C}$, and (d) $\dot{m} = 60 \text{ kg/s}$ and $T_{inj} = 80^{\circ}\text{C}$.

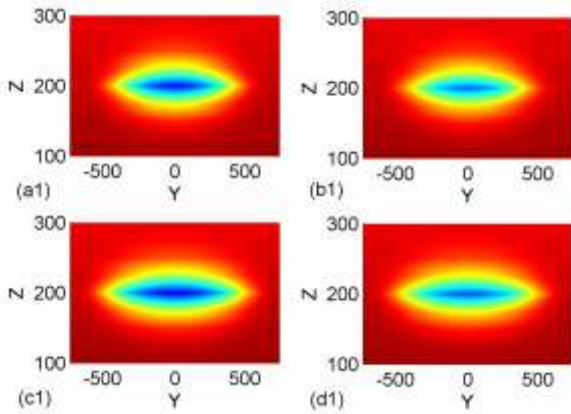


Fig. 9. The zoom views of temperature fields of Fig. 8.

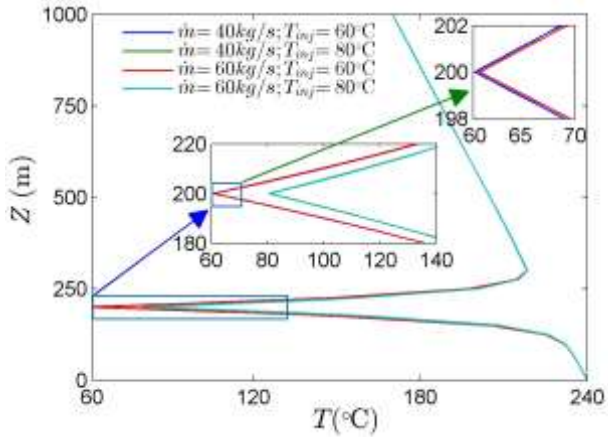


Fig. 10. The temperature profile in vertical direction at injection point after 20 years.

The vertical temperature distributions inside the low permeable rock matrix for Cases 1-4 are shown in Figs. 6 and 8 (zoom view in figs. 7 and 9). Figs. 6 and 8 shows that the temperature drop inside the rock matrix occurred less than 100 m from the fracture. For very small value of matrix permeability, the heat transfer inside the inside the rock matrix is only by the conduction. Comparing the all Cases, it is seen that slightly more temperature drop occurs in vertical directions for Case 3 because in this case the colder fluid is injection with higher mass flow rate. The temperature profiles along the vertical line passing through the injection well are shown in Fig. 10 for Case 1-4. Near the fracture, almost linear temperature profile is observed. However approximately 100 m away from the fracture, the temperature profile match the initial geothermal gradient.

In Fig. 11, the variation of production temperature, heat extraction rate, power output and injectivity with time are plotted. The early thermal breakthrough and faster

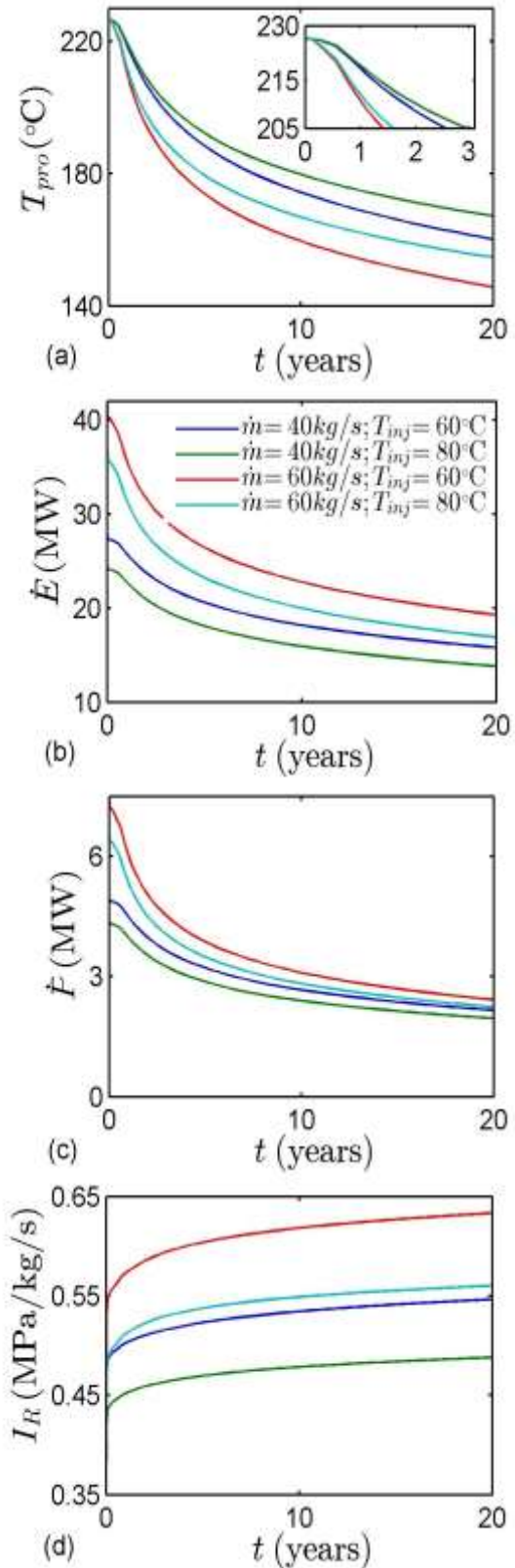


Fig. 11. Comparison of results to show the effect of different injection mass flow rate and injection temperature on the variation of (a) temperature, (b) heat extraction rate, (c) electric power output, and (d) flow impedance.

temperature drop at production well is caused by the slow heat transfer rate from the low permeable rock matrix at the interface. Due to the faster cooling of fracture by strong advection and slow conduction in the rock matrix, the fluid in fracture did not get enough time to capture the heat from the low permeable rock matrix. But at later stage production temperature decreases slowly and heat transfer from the rock matrix reaches steady state in parts of the fracture. The temperature breakthrough at production well occur early for higher mass flow rate at lower injection temperature. The heat extraction rate and electric power output with time for all cases are presented in Figs. 11b-11c. Figs. 11b and 11c show that heat extraction rate and electric power output is comparably more for Case 3, due to higher mass injection at low injection temperature. However, the lower injection temperature help to extract more energy from the reservoir. For the higher injection temperature, heat extraction rate decreases due to the less temperature difference between injected fluid and rock/fracture. Fig. 11d shows the evolution of the reservoir impedance (flow impedance) with time for all injection scenarios. Fig. 11d shows that increasing the mass flow rate from 40 to 60 kg/s results in a increase of flow impedance. This is because of higher mass flow rate increased the flow resistance. Fig. 11 d also shows that increasing the injection temperature reduces the flowing impedance. In this case flow resistance is decreased due to lower fluid viscosity.

6. Conclusion

In this study, a three-dimensional coupled Thermo-Hydro model of geothermal heat extraction has been presented. Series of numerical simulations comprising of different injection temperature (T_{inj}) and mass flow rate (\dot{m}) were carried out to analyze their effects on the heat extraction performance, energy output and flow impedance changes from a fractured geothermal reservoir. It was observed that the injection temperature and mass flow rate have a profound effects on temperature drawdown at the production well and cooling of fracture/matrix system. The result of higher injection mass at lower temperature shows faster drop of temperature at the production well and relatively early thermal breakthrough. But, in this case, more heat extraction from the reservoir due to greater utilization of available resource. The results also showed that the flow impedance rises due to the increase of viscosity as the result of temperature drop inside the reservoir. The flow impedance of reservoir was less for higher injection temperature. However, in that scenario both power output and heat extraction rate decreased.

References

- [1] B. B., R. Saim, H. Benzenine, H. F. Oztop, "Analysis of thermal and dynamic compoment of a geothermal vertical U-tube heat exchanger", Energy and Buildings, vol. 58, pp. 37-43, 2013.
- [2] B. D. P. Hepburn, M. Sedighi, H. R. Thomas, Manju, "Field-scale monitoring of a horizontal ground source heat system", Geothermics, vol. 61, pp. 86-103, 2016.
- [3] A. S. Kord and S. S Jazayeri, "Optimization and Analysis of a Vertical Ground-Coupled Heat Pump", International journal of renewable energy research, vol. 2 (1), pp. 33-37, 2012.
- [4] J.W. Lund, T.L. Boyd, "Direct utilization of geothermal energy 2015 worldwide review", Geothermics, vol 60, pp. 66-93, 2016.
- [5] R. Bertani, "Geothermal power generation in the world 2010-2014 update report", Geothermics, vol. 60, pp. 31-43, 2016.
- [6] IEA-Technology Roadmap Geothermal Heat and Power. International Energy Agency. http://www.iea.org/publications/freepublications/publication/Geothermal_roadmap.pdf.
- [7] M. Deo, R. Roehner, R. Allis, J. Moore, Modeling of geothermal energy production from stratigraphic reservoirs in the Great Basin", Geothermics, vol. 51, pp. 38-45, 2014.
- [8] S. Finsterle, Y. Zhang, L. Pan, P. Dobson, K. Oglesby, "Microhole arrays for improved heat mining from enhanced geothermal systems", Geothermics, vol. 47, pp. 104-115, 2013.
- [9] S.N. Pandey, A. Chaudhuri, S. Kelkar, VR Sandeep, H. Rajaram, "Investigation of permeability alteration of fractured limestone reservoir due to geothermal heat extraction using three-dimensional thermo-hydro-chemical (THC) model", Geothermics, vol. 51, pp. 46-62, 2014.
- [10] C. Rawal and A. Ghassemi, "A reactive thermo-poroelastic analysis of water injection into an enhanced geothermal reservoir", Geothermics, vol. 50, pp. 10-23, 2014.
- [11] Y. Zhao, Z. Feng, Z. Feng, D. Yang, W. Liang, "THM (Thermo-hydro-mechanical) coupled mathematical model of fractured media and numerical simulation of a 3D enhanced geothermal system at 573 K and buried depth 6000-7000 M", Energy, vol. 82, pp. 193-205, 2015.
- [12] Y. Zeng, J. Zhan, N. Wu, Y. Luo, W. Cai, "Numerical investigation of electricity generation potential from fractured granite reservoir by water circulating through

- three horizontal wells at Yangbajing geothermal field", *Applied Thermal Engineering*, vol. 104, pp. 1-15, 2016.
- [13] S. Held, A. Genter, T. Kohl, T. Kölbl, J. Sausse, M. Schoenball, "Economic evaluation of geothermal reservoir performance through modeling the complexity of the operating EGS in Soultz-sous-Forêts", *Geothermics*, vol. 51, pp. 270-280, 2014.
- [14] F. Jiang, L. Luo, J. Chen, "A novel three-dimensional transient model for subsurface heat exchange in enhanced geothermal systems", *International Communications in Heat and Mass Transfer*, vol. 41, pp. 57-62, 2013.
- [15] F. Jiang, J. Chen, W. Huang, L. Luo, "A three-dimensional transient model for EGS subsurface thermo-hydraulic process, *Energy*", vol. 72, pp. 300-310, 2014.
- [16] T. Hadgu, E. Kalinina, T. S. Lowry, "Modeling of heat extraction from variably fractured porous media in Enhanced Geothermal Systems", *Geothermics*, vol. 61, pp. 75-85, 2016.
- [17] Don B. Fox, Daniel Sutter, Koenraad F. Beckers, Maciej Z. Lukawski, Donald L. Koch, Brian J. Anderson, Jefferson W. Tester, "Sustainable heat farming: Modeling extraction and recovery in discretely fractured geothermal reservoirs", *Geothermics*, vol. 46, pp. 42-54, 2013.
- [18] E. Kalinina, S. A. McKenna, T. Hadgu, "Thomas Lowry Analysis of the effects of heterogeneity on heat extraction in an EGS represented with the continuum fracture model", *Proceedings, Thirty-Seventh Workshop on Geothermal Reservoir Engineering Stanford University, Stanford, California, SGP-TR-194, January 30 February 2012.*
- [19] N. Bagalkot and G. Kumar, "Thermal front propagation in variable aperture fracture–matrix system: A numerical study" *Sadhana*, vol. 40, pp. 605-622, 2015.
- [20] S.N. Pandey, A. Chaudhuri, H. Rajaram and S. Kelkar, "Fracture transmissivity evolution due to silica dissolution/precipitation during geothermal heat extraction", *Geothermics*, vol. 57, pp. 111-26, 2015.
- [21] C. Xu, P. A. Dowd, Z. F. Tian, "A simplified coupled hydro-thermal model for enhanced geothermal systems". *Applied Energy*, vol. 140, pp. 135-45, 2015.
- [22] P. Ortoleva, M. Enrique, C. Moore, J. Chadam, "Geochemical self-organization I; reaction-transport feedbacks and modeling approach", *Am. J. Sci.*, vol. 287, pp. 979-1007, 1987.
- [23] R. Blair Hanna and H. Rajaram, "Influence of aperture variability on dissolutional growth of fissures in Karst Formations", *Water Resources Research*, vol. 34, pp. 2843–53, 1998.
- [24] A. Chaudhuri, H. Rajaram, H. Viswanathan, "Alteration of fractures by precipitation and dissolution in gradient reaction environments: computational results and stochastic analysis", *Water Resour. Res.*, vol. 44, W10410, <http://dx.doi.org/10.1029/2008WR006982>, 2008.
- [25] R.W. Zimmerman, A. Al-Yaarubi, C.C. Pain, C. A. Grattoni, "Nonlinear regimes of fluid flow in rock fractures", *Int. J. Rock Mech. Min. Sci.*, vol. 41, pp. 384, 2004.
- [26] G. Zyvoloski, "FEHM: a control volume finite element code for simulating subsurface multi-phase multi-fluid heat and mass transfer", May 18. In: *Technical report LAUR-07-3359*, 2007
- [27] S. Kelkar, K. Lewis, S. Karra, G. Zyvoloski, S. Rapaka, H. Viswanathan, P.K. Mishra, S. Chu, D. Coblenz, R. Pawar, "A simulator for modeling coupled thermo-hydro-mechanical processes in subsurface geological media. *International Journal of Rock Mechanics and Mining Sciences*, vol. 70, 569-80, 2014.
- [28] S. K. Sanyal and S. J. Butler, "An analysis of power generation prospects from enhanced geothermal systems", *Transactions Geothermal Resources Council*, vol. 29, pp. 131–138, 2005.